Hayder A. Dhahad
Training and Workshop Centre,
University of Technology,
Baghdad, Iraq
e-mail: 10592@uotechnology.edu.iq

Gazy F. Al-Sumaily[1]
Training and Workshop Centre,
University of Technology,
Baghdad, Iraq;
Fluids Laboratory for Aeronautical and Industrial
Research (FLAIR),
Department of Mechanical and Aerospace
Engineering,
Monash University,
Victoria 3800, Australia,
e-mails: gazy.alsumaily@uotechnology.edu.iq;
gazy.alsumaily@monash.edu

Laith J. Habeeb
Training and Workshop Centre,
University of Technology,
Baghdad, Iraq
e-mail: laithhabeeb1974@gmail.com

Mark C. Thompson
Fluids Laboratory for Aeronautical and Industrial
Research (FLAIR),
Department of Mechanical and Aerospace
Engineering,
Monash University,
Victoria 3800, Australia
e-mail: mark.thompson@monash.edu

The Cooling Performance of Mixed Convection in a Ventilated Enclosure With Different Ports Configurations

Mixed convection heat transfer in a vertically oriented air-cooled square enclosure is simulated numerically using the finite volume method. The vertical left wall being heated and all others are considered insulated. The effects of six opposite and staggered inlet/ outlet openings' locations over the top and bottom walls are investigated, with different sizes of the opening height ($0.05 \leq d/H \leq 0.3$). The objective is to figure out the better size and location of inlet and outlet to acquire more efficient cooling system in the enclosure by maximizing the heat removal rate. This is conducted over ranges of the governing parameters, which are the Richardson number ($0 \leq Ri \leq 30$) and the Reynolds number ($50 \leq Re \leq 250$). The results show that the level of heat transfer enhancement increases with increasing the opening height, with an optimal size of $d/H = 0.25$ for obtaining maximum heat removal, for all Richardson and Reynolds numbers. The results also indicate that the higher heat dissipation occurs when the cold air is injected vertically near the hot wall and exits the enclosure from the opposite or staggered outlet, for all Richardson and Reynolds numbers. [DOI: 10.1115/1.4048096]

Keywords: mixed convection, aiding and opposing laminar flows, ventilated enclosure

1 Introduction

The common fields of application of fluid flow and heat transfer resulting from the combined influence of free and forced convection is in designing cooling systems for electronic equipment such as computers. In such equipment, a small heat source is generally placed inside an enclosure and is subjected to a specified heat flux. Thus, the interaction between the buoyancy driven flow induced by the heat flux and the external forced cooling flow may lead to the possibility of complicated flows. Several enclosure orientations, ventilation systems, and/or heating conditions of the enclosure can stimulate different types of buoyant flows that may augment the heat transfer in different ways. For example, for combined convection in a vertical enclosure, when the buoyancy is insignificant, modest buoyant flows motivate along the hot wall and might either resist or assist the mainstream and cause either small reduction or augmentation in the heat transfer. However, when the buoyancy turns into significant, the generated buoyant flows become robust and can cause different sorts of flow reversals that can change considerably the whole flow and thermal characteristics inside the enclosure. Indeed, this kind of secondary flow that could have a switch into a two-dimensional convection cells based on the values of the buoyancy parameter and the Reynolds number, as well as on the orientation of the ventilation system and the initial and final positions of the main flow.

For the case of mixed convection in a horizontally oriented ventilated enclosure [1] presented quantitative results on mixed convection transport inside a square enclosure for different displacement configurations by changing the location of the outflow opening and the finite size heat source. The results showed that when the inflow opening and the heat source are located on the same enclosure vertical left wall, the higher location of the source leads to a better cooling effect. An enhancement in the cooling is also achieved when the outflow opening is located close to the lowest of the opposite vertical right wall. However, once the source is placed at the floor of the enclosure, the cooling becomes more efficient when the outflow opening is placed close to the middle and far of the inlet. Papanicolaou and Jaluria [2] reported the transition from a steady, laminar-mixed convection regime to a periodic regime in an air-filled enclosure induced by localized heating. They found that the interaction between the buoyancy-induced flow with the cold through-flow might become unstable beyond a critical value of the mixed convection parameter; hence, after an initial transient, very regular, periodic, almost sinusoidal oscillatory behaviors were shown for the results. Hsu et al. [3] investigated mixed convection in a partially divided rectangular enclosure with a finite size heat source. The enclosure is partially divided by a vertical divider protruding from the ceiling or the floor of the enclosure. The impacts of the height and place of the divider, and the locations of the outflow opening and the heat source, were examined. They stated that the better cooling performance could be achieved by placing the heat source in the vicinity of the cold inlet port and/or by locating the outflow opening lower of the vertical right wall.

Laminar combined free and forced convection in a horizontal air-cooled rectangular enclosure comprising radiation from the

left sidewall by Raji and Hasnaoui [4] and from the left side and top walls by Raji and Hasnaoui [5]. They considered two enclosure configurations: bottom–top (BT) and bottom–bottom (BB) configurations. It was found that the BB configuration is unfavorable and not beneficial for heat removal, as it results in higher values of the mean temperature within the enclosure. Lee et al. [6] studied the characteristics of turbulent and laminar mixed convection flows in an rectangular air-cooled enclosure. They investigated only one the top–bottom (TB) flow configuration, where air is inserted at the upper part of the left vertical hot wall and permitted to quit at the lower part of the right vertical cold wall. The results showed that the air-cooling is not efficient in laminar mixed convection as the heat transfer becomes predominant over the convective heat transfer, and the buoyancy forces induce heat energy from the heat source into the enclosure. Later, the same TB flow configuration was also investigated by Moraga and Lopez [7] and most recently by Doghmi et al. [8] but for a three-dimensional model. They captured and presented the velocity
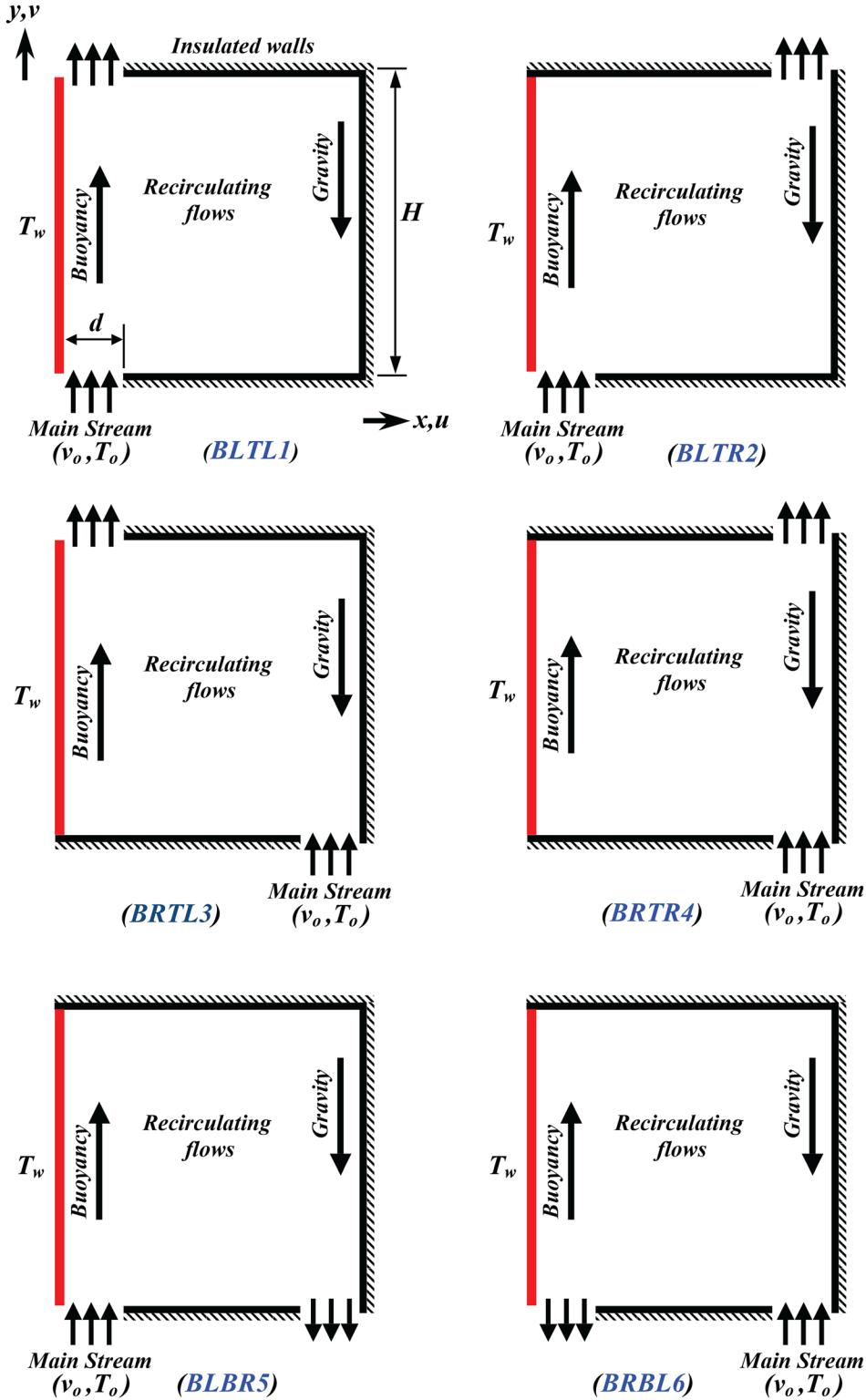
Fig. 1 Physical configuration with system coordinates

profiles and the rates of heat removal in a rectangular TB air-ventilated enclosure for wide ranges of Reynolds and Richardson numbers and for different sizes of inlet opening. Their results demonstrated that the flow strength and the amount of heat released could be considerably enhanced by the best selection for the mentioned parameters. Omri and Ben Nasrallah [9] investigated transient laminar mixed convection in an enclosure with two vertical walls kept at different constant temperatures and two horizontal insulated walls by considering two different air injection configurations; TB and BT. It was revealed that the air-cooling is more effective when Reynolds number exceeds a critical value for a given Richardson number, and the BT air injection configuration is more effective for heat removal. Later on, Singh and Sharif [10] extended the work of Omri by studying six different configurations of inlet/outlet placements to identify the optimum one for obtaining higher air-cooling efficiency within a differentially heated rectangular enclosure. They observed that the most cooling effectiveness is attained by locating the inlet vent close the bottom of the cold wall, and the outlet exit close the top of the hot wall.

Rahman et al. [11] studied the influence of 19 inlet port locations on the opposing mixed convection and heat transfer for ranges of Richardson, Reynolds, and Prandtl numbers in a square-vented enclosure. They indicated that the increase in Reynolds number leads to higher Nusselt number and higher intensity of recirculation, and the heat transfer rates depend significantly on the position of the inlet port. Bahlaoui et al. [12] reported results of coupled mixed convection and radiation within a horizontal BT-ventilated enclosure heated from below and provided with an adiabatic partition on the hot floor. They found that the heat transfer enhances by increasing the displacement of the partition away from the inlet opening. Their results displayed unsteady periodic solution for a particular position of the partition. Oztop [13] examined mixed convective flows in a rectangular enclosure with volumetric heat sources. The study investigated the effect of three locations of the exit opening; single opening near the ceiling, single opening near the bottom, and double openings. The greatest heat transfer was found to be once the opening of outlet is placed onto top of the right vertical wall near the ceiling. Nosonov and Sheremet [14] studied conjugate mixed convection heat transfer in a horizontal square cavity having solid walls of finite thickness and conductivity under the influence of local heaters. The results revealed that the increase in Richardson number strengthens the intensity of the internal convective vortex that distorts the forced stream-flow.

In contrast, for the case of mixed convection in a vertically oriented ventilated enclosure, the results are rather limited. Sparrow and Samie [15] made a numerical analysis of combined convective flow in a vertical cylindrical enclosure throughout small apertures centered in the lower and upper surfaces. The buoyancy forces are induced in the enclosure due to the temperature discrepancy between the penetrating fluid and the enclosure walls. They noted that when the flow-stream is vertically upward, the small and intermediate amount of natural convection causes a reducing in the heat dissipation; however, high values of heat dissipation can be resulted when the natural convection is overpowered. Nevertheless, for vertically downward flow-stream, the flow field in the enclosure is basically unaltered and the heat transfer is slight changed from that for nonbuoyant flow. Oosthuizen and Paul [16] studied assisting and opposing mixed convective flows in a rectangular vertical enclosure with the right and left vertical walls heated and cooled, respectively, and the remaining two horizontal walls adiabatic. Their attention was given to the case where the forced flow enters and exits the enclosure throughout the cold left wall and the entering fluid has the same temperature as the cold wall. It was shown that the buoyancy forces increase the rates of heat transfer in aiding flows, whereas in opposing flows they decrease it at higher Reynolds numbers but increase it when the purely free convective becomes predominant at low Reynolds numbers. Kumar and Yuan [17] also examined the effect of aiding and opposing buoyancy forces on the flow and thermal structures of mixed convection flow in a vertical rectangular enclosure for a range of Reynolds and Richardson numbers. However, their flow configuration was different: The vertical hot or cold downward jet enters the enclosure from the ceiling at one end of the top corner and discharges through the ceiling at the other top corner. The positive and negative buoyancies in this kind of flow configuration were found to be significantly impact the velocity and temperature distributions and the convective heat transfer coefficient. Angirasa [18] presented numerical results for mixed convection heat transfer in a vertical square enclosure with an entry slot and an outlet vent located, , respectively, at the bottom and the top edges of the vertical left hot wall, while keeping the remaining three walls insulated. The intricate interaction between the positive and negative buoyancy effects and the forced flow for different Grashof and Reynolds numbers was investigated. It was identified that at lower Grashof number, the heat transfer augments with increasing Reynolds number for either vertically upward or downward direction of the buoyancy. However, for higher Grashof number, when the buoyancy acts vertically upward, the interaction between the
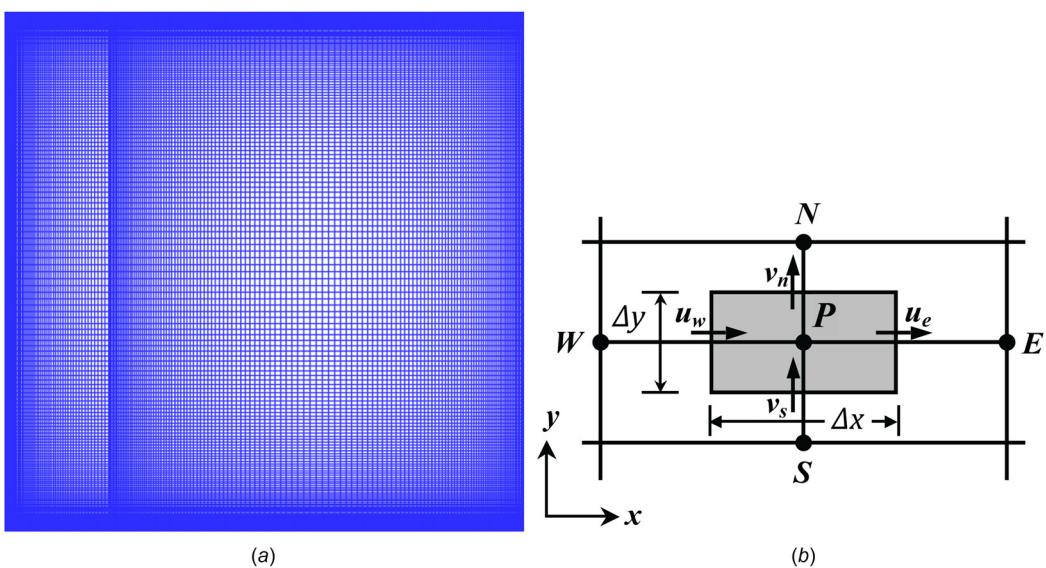
Fig. 2 (*a*) The computational grid used for the (BLTL1) configuration and (*b*) typical control volume showing the main and staggered grids

Table 1 Grid sizes used to check the grid independency

Mesh	$(\Delta x \times \Delta y)$
M1	(102×102)
M2	(136×136)
M3	(170×170)
M4	(204×204)
M5	(238×238)
M6	(272×272)

two flow mechanisms was found to become quite sophisticated and the steady-state solutions could not be determined.

Indeed, even when the effects of the natural convection are trivial, i.e., for small Richardson numbers, the predictable patterns of fluid motion during an enclosure are much complicated due to producing a large-scale vortex along the walls of the enclosure. For higher heating (higher Richardson numbers), the forces of the buoyant convective flow interact with the foregoing vortex, and may interact with the main stream-flow causing this primary eddy. Therefore, for a specified value and location of the main stream-flow (Reynolds number), it is interesting to distinguish the Richardson numbers at which these extremely sophisticated interactions take place. This study is a

further investigation to the work carried out by Angirasa [18], where only one possible placement configuration of the inlet and outlet openings was investigated. In the present investigation, several other possible placements (an overall of six enclosure configurations) of the inlet and outlet, containing this of [18], are considered for broad ranges of Reynolds and Richardson numbers. The six enclosure configurations studied, namely, bottom-left-top-left (BLTL1), bottom-left-top-right (BLTR2), bottom-right-top-left (BRTL3), bottom-right-top-right (BRTR4), bottom-left-bottom-right (BLBR5), and bottom-right-bottom-left (BRBL6), are illustrated in Fig. 1. The physical model is a basic geometry of a square enclosure, vertically oriented; with two same-size (d) inlet and outlet ports. The figure portrays that the fluid stream enters the enclosure via the inlet port, which is always located in the bottom, with a velocity (v_o) and a temperature (T_o) and exits via the outlet port. The left vertical wall of the enclosure is isothermally heated and kept at a constant temperature (T_w), while the other walls are assumed to be insulated. Attention is only given to the case where $T_w > T_o$ (cooling system). Thus, the objective of this study is to recognize the preferable inlet and outlet placement configuration to secure most effective cooling, and to understand the flow and thermal structures of assisting and opposing mixed convective flows inside the vertical enclosure for various values of the above parameters. The size effect of the inlet/outlet openings (d/H) is also investigated.
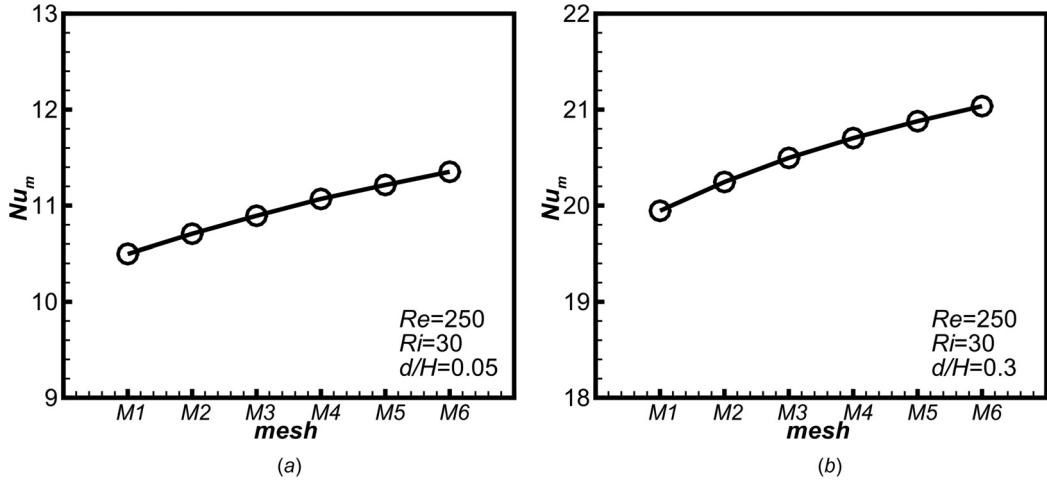
Fig. 3   Results of Nu_m for the GRS: (a) at Re = 250, Ri = 30, d/H = 0.05 and (b) at Re = 250, Ri = 30, d/H = 0.3
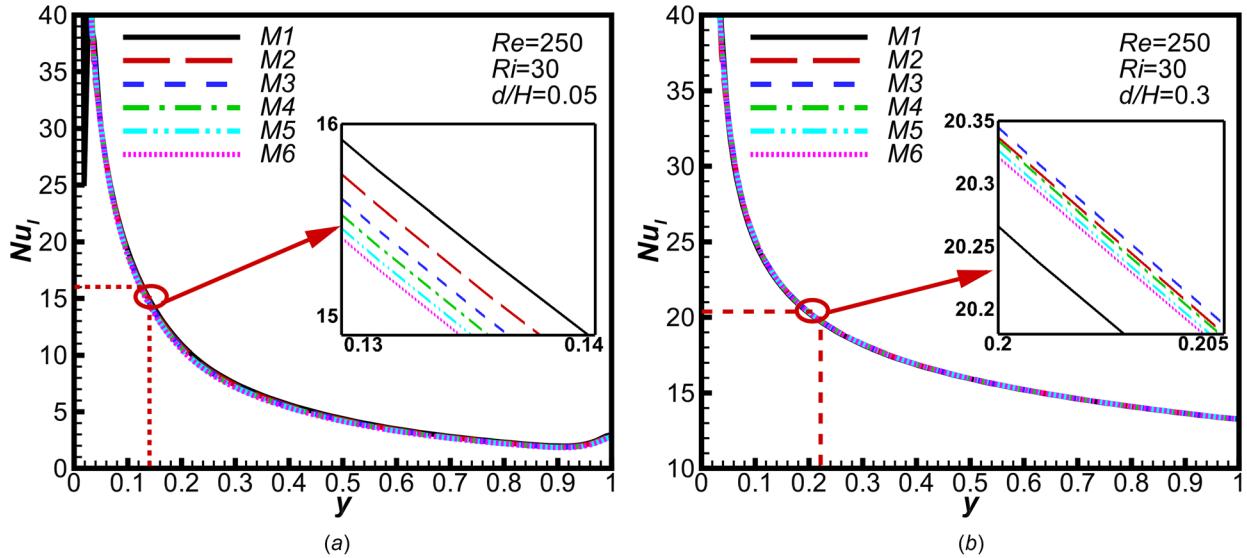
Fig. 4   Results of Nu_l for the GRS: (a) at Re = 250, Ri = 30, d/H = 0.05 and (b) at Re = 250, Ri = 30, d/H = 0.3
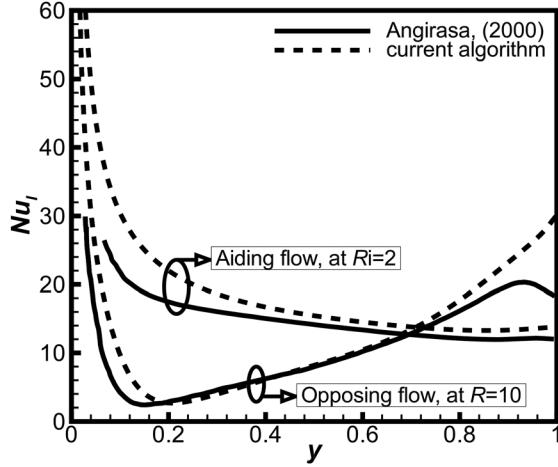
Fig. 5 The comparison between two numerical models: The current algorithm and that employed by [18] for the mixed convection flow in an enclosure, for the variation of Nu_l of aiding flow at Ri = 2 and opposing flow at Ri = 10

2 Mathematical Formulation

The considered cooling fluid is air with a Prandtl number of ($Pr = 0.71$), and the flow is assumed unsteady, laminar, and incompressible with negligible viscous dissipation. All the thermophysical properties of the fluid are assumed constant except the density change with temperature, giving rise to the buoyancy forces, which is treated as usual by means of the Boussinesq approximation. The governing equations for the two-dimensional, transient, laminar, and incompressible fluid can be expressed in the following dimensionless form:

$$\nabla \cdot \mathbf{u} = 0 \tag{1}$$

$$\frac{\partial \mathbf{u}}{\partial t} + \mathbf{u} \cdot (\nabla \mathbf{u}) = \frac{1}{Re}(\nabla^2 \mathbf{u}) - \nabla P + S_\theta \tag{2}$$

$$\frac{\partial \theta}{\partial t} + \mathbf{u} \cdot (\nabla \theta) = \frac{1}{Re \cdot Pr}(\nabla^2 \theta) \tag{3}$$

where ($\mathbf{u}$) is the velocity vector field, while (P), (t), and (θ) represent the dimensionless pressure, time, and temperature, respectively. S_θ is the source term in the momentum equations; ($S_\theta = 0$) in the x-momentum equation and ($S_\theta = Ri \cdot \theta$) in the y-momentum equation. It can be seen that the problem is regulated by four main dimensionless parameters: Two of them identify the flow of the fluid, the main stream-flow Reynolds number (Re), and the natural convection, the Richardson number (Ri), in the enclosure. Another two are geometrical parameters: The ratio of the opening size to the enclosure height (d/H) and the location of the inlet/outlet openings (displacement configurations). The Reynolds and Richardson numbers are defined as:

$$Re = \frac{v_o H}{\nu}, \quad Ri = \frac{Gr}{Re^2}, \quad Gr = \frac{g \cdot \beta \cdot H^3 (T_w - T_o)}{\nu^2}$$

where (Gr) is the Grashof number, (ν) is the kinematic viscosity, with (g) and (β) are the gravitational acceleration and the volumetric expansion coefficient, respectively. The nondimensional boundary conditions applied for the present problem are
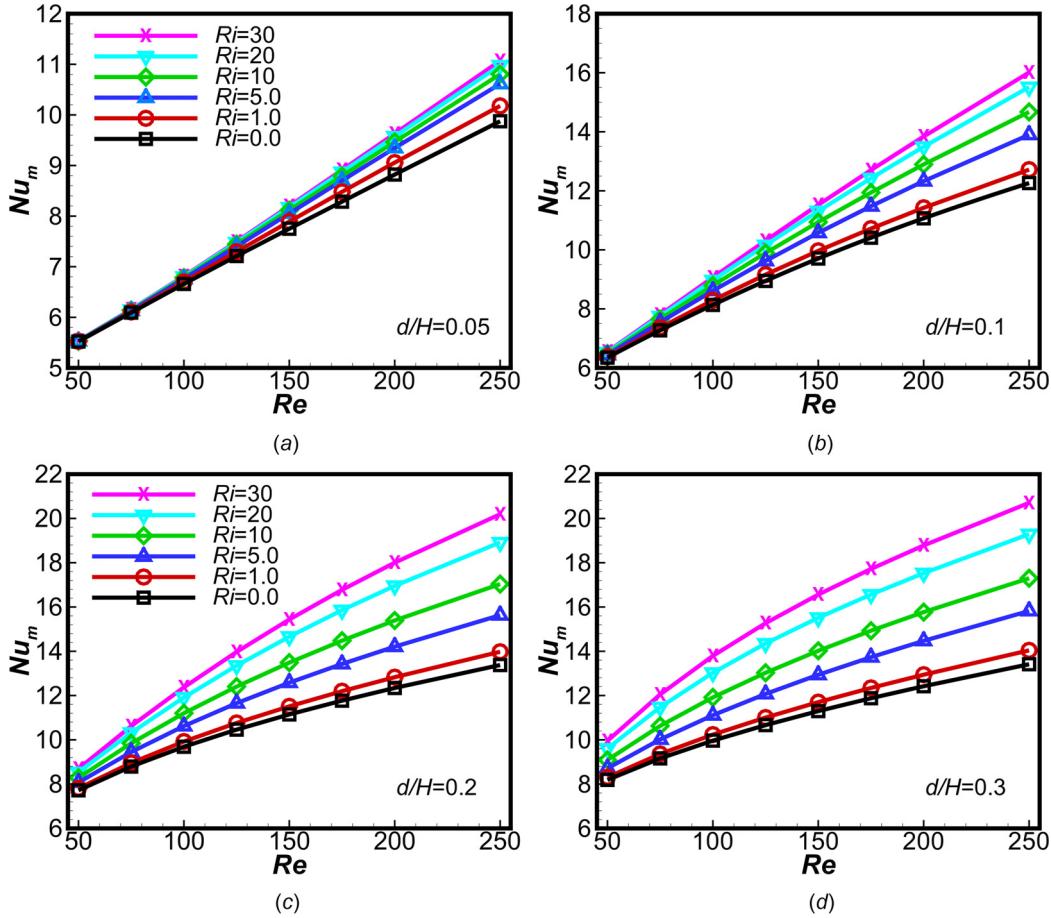
Fig. 6 Variation of Nu_m with Re for different Ri and d/H: (*a*) at $d/H = 0.05$; (*b*) at $d/H = 0.1$; (*c*) at $d/H = 0.2$; and (*d*) at $d/H = 0.3$

$u_o = 0,$ $v_o = 1$ and $\theta_o = 0$ at the inlet

$\dfrac{\partial u}{\partial y} = \dfrac{\partial v}{\partial y} = \dfrac{\partial \theta}{\partial y} = 0$ at the exit

$u_w = v_w = 0$ and $\theta_w = 1$ at the heated vertical left wall

$u = v = 0$ and $\dfrac{\partial \theta}{\partial x} = 0$ at the insulated vertical right wall

$u = v = 0$ and $\dfrac{\partial \theta}{\partial y} = 0$ at the insulated horizontal walls

The rate of heat transfer from the vertical left wall is computed and expressed in terms of the surface-average Nusselt number (Nu_m) and the local Nusselt number (Nu_l) as

$$Nu_l = \dfrac{\partial \theta}{\partial n}\bigg|_w, \quad Nu_m = \dfrac{1}{H}\sum\int_0^H Nu_l \cdot dn \qquad (4)$$

where n is the normal direction with respect to the wall.

3 Numerical Procedure

The method of finite volume developed by Patankar [19] was incorporated in a home-developed FORTRAN code to numerically discretize and solved the nondimensional governing Eqs. (1)–(3). The first step is to divide the computational domain entirely into vertical and horizontal nonuniformly spaced grid
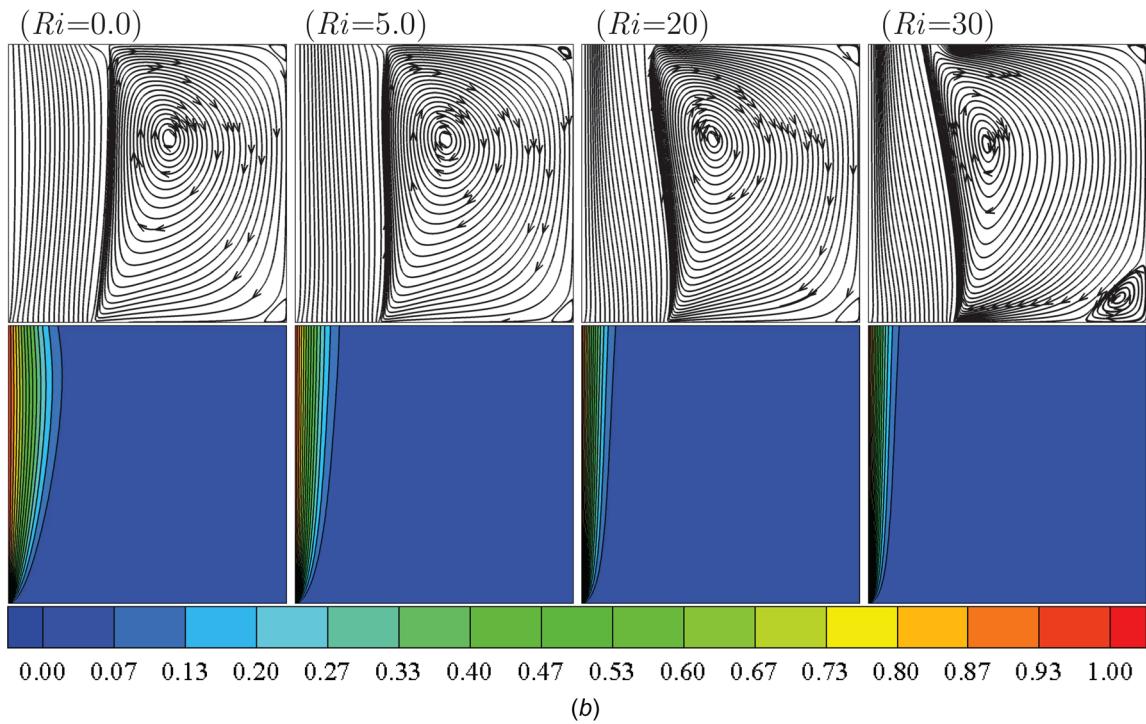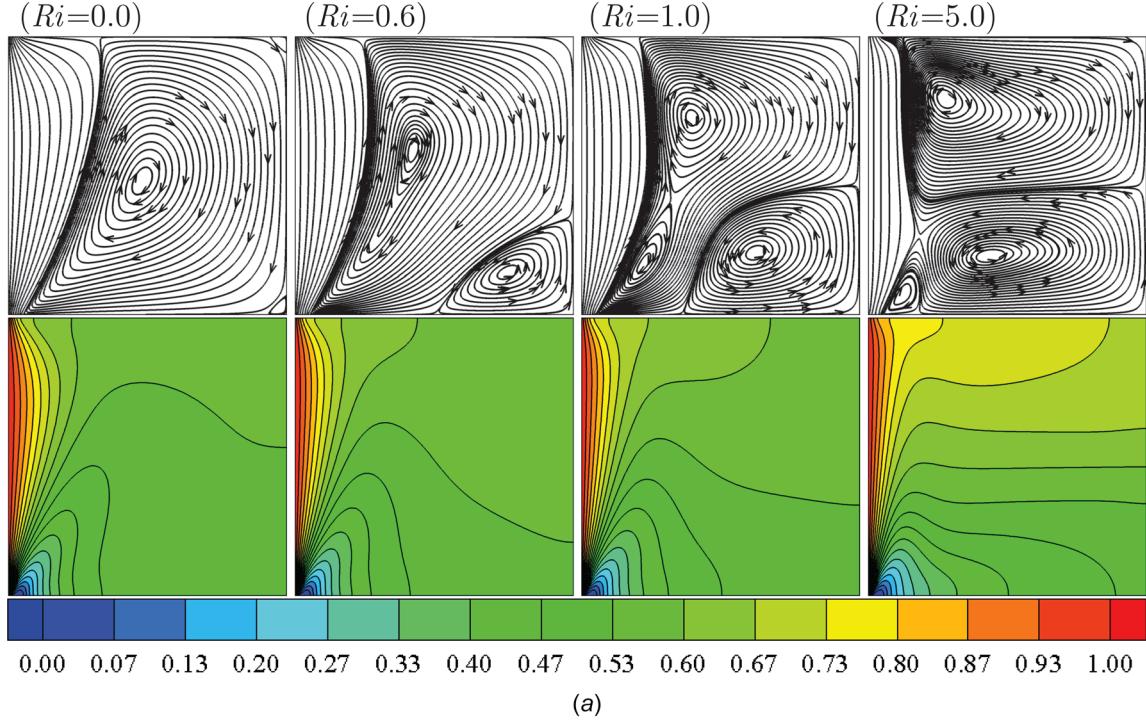
Fig. 7   Effect of Ri on the streamlines and isotherms, for (*a*) *d/H* = 0.05 and (*b*) *d/H* = 0.3, at Re = 250

lines, as illustrated in Fig. 2(a) for the (BLTE1) enclosure configuration at $d/H = 0.2$. The grid spacing is nonuniform in both directions to allowing fine grid lines in the regions with sharp gradients such as near walls. The intersection of the grid lines form the so-called grid nodes, each of which is assumed to be surrounded with a control volume. The boundaries of the control volume are taken to be in the midway between the grid nodes. All scalar-dependent variables such as pressure and temperature are stored in the grid nodes, while the components of the velocity are stored at staggered locations coinciding with the boundaries of the control volumes for the scalar variables. The adoption of these staggered locations ensures that the velocities lay between the pressures that induce them, and are available directly for computing the convective fluxes of the scalar flow variables. A typical control volume ($\Delta x \times \Delta y$) around a point P communicating with four neighboring grid points E, W, N, S, and the staggered locations for the velocity components at the four faces of the control volume are shown in Fig. 2(b). The governing differential Eqs. (1)–(3) are then integrated over each finite control volume using the Hybrid differencing scheme detailed in the study by Ferziger and Peric [20] for approximating nonlinear discretization algebraic equations. The SIMPLEC algorithm of [19] is used to couple the momentum and continuity approximations, and then to iteratively solve them over the whole control volumes using the alternating direction implicit
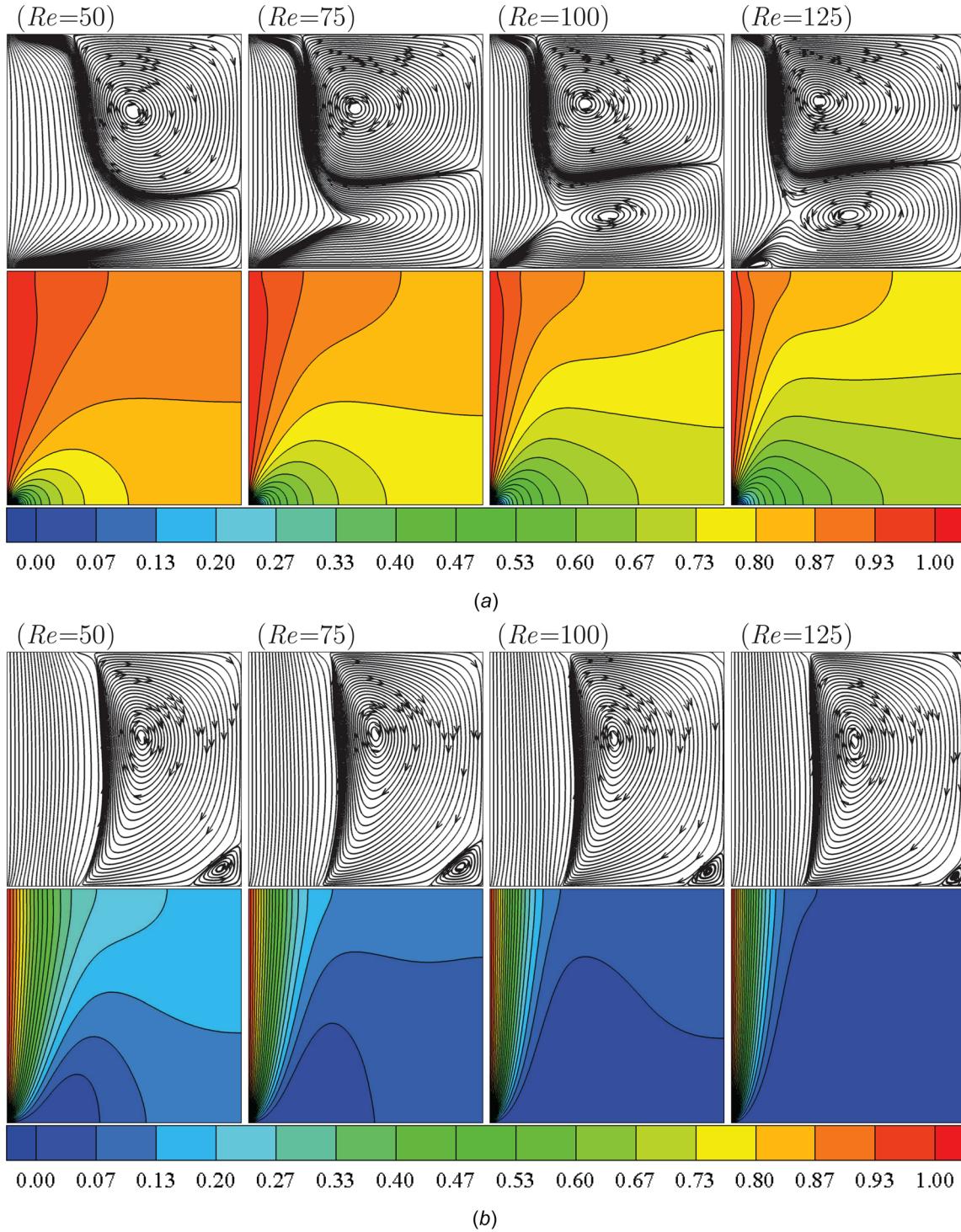
Fig. 8 Effect of Re on the streamlines and isotherms, for (a) $d/H = 0.05$ and (b) $d/H = 0.3$, at Ri = 5.0

(ADI) method, describing the distributions of the dependent variables at the grid points. The accuracy of the predicted results is assessed by ensuring sufficiently small residuals for all variables solved everywhere in the field are reduced to an acceptable level using a convergence criteria. To facilitate monitoring the convergence of the numerical solution, the calculated local and surface-average Nusselt numbers Nu_l and Nu_m are observed as accuracy indication. The value of convergence criteria adopted for this study is typically less than (10^{-6}).

3.1 Numerical Code and Grid Size Validations. A grid resolution study (GRS) was conducted to check the solution grid independency employing variant nonuniform sizes $M1$, $M2$, $M3$, $M4$, $M5$, and $M6$, as demonstrated in Table 1. The GRS was undertaken for many smallest and largest values of the pertinent parameters. Sample of results for the preliminary tests is illustrated in Figs. 3 and 4. The average and local Nusselt numbers Nu_m and Nu_l, respectively, were also monitored in this study to determine the convergence. The computational domain $M4$ was chosen to be suitable for this study since it allows a decent compromise between the computational charge and the precision of the acquired results with a maximum deviation at 0.5%. For the validation of the numerical scheme, some calculations were made to compare the simulated results with the other simulated results available in the literature and reported by Angirasa [18] considering the problem of mixed convection in an enclosure. Figure 5 shows the comparison of the variation of local Nusselt number Nu_l of aiding flow at $Ri = 2$ and of opposing flow at $Ri = 10$. As shown from the figure that the comparison of results is acceptable.

4 Results and Discussion

As mentioned in Sec. 1, the attention will be given here to the influences of the fluid flow considerations such as Reynolds (Re) and Richardson numbers (Ri), and to the geometrical considerations such as the enclosure inlet/outlet openings size and locations. Correspondingly, Reynolds number changes within the range of ($50 \leq \mathrm{Re} \leq 250$) in the calculations, the Richardson number was varied systematically from 0 (forced convection) to 30 (high heating), within six enclosure displacement configurations, e.g., BLTL1, BLTR2, BRTL3, BRTR4, BLBR5, and BRBL6. Also, six values of the openings size ($d/H = 0.05$, 0.1, 0.15, 0.2, 0.25, 0.3) were used only during the first BLTL1 configuration. For all cases, Prandtl number equals to ($\mathrm{Pr} = 0.71$) is used.

4.1 Effect of Reynolds and Richardson Numbers. The effect of Reynolds number on the average Nusselt number (Nu_m) for different values of Richardson number $Ri = 0$, 1, 5, 10, 20, and 30, in the BLTL1 displacement configuration at four values of openings size $d/H = 0.05$, 0.1, 0.2, and 0.3, is shown in Figs. 6(a), 6(b), 6(c), and 6(d), respectively. The figures reveal an enhancement in the heat transfer as Reynolds number and/or Richardson number increase. It is found that Nu_m increases sharply and linearly by increasing Reynolds number at the smallest opening port $d/H = 0.05$; however, for $d/H > 0.1$, the increase in Nu_m becomes gradual and nonlinear. It can be observed that the influence of increasing Richardson number is more significant for higher opening size and higher Reynolds number because of the inlet and the outlet openings are very close from the heat source in the (BLTL1) flow configuration.
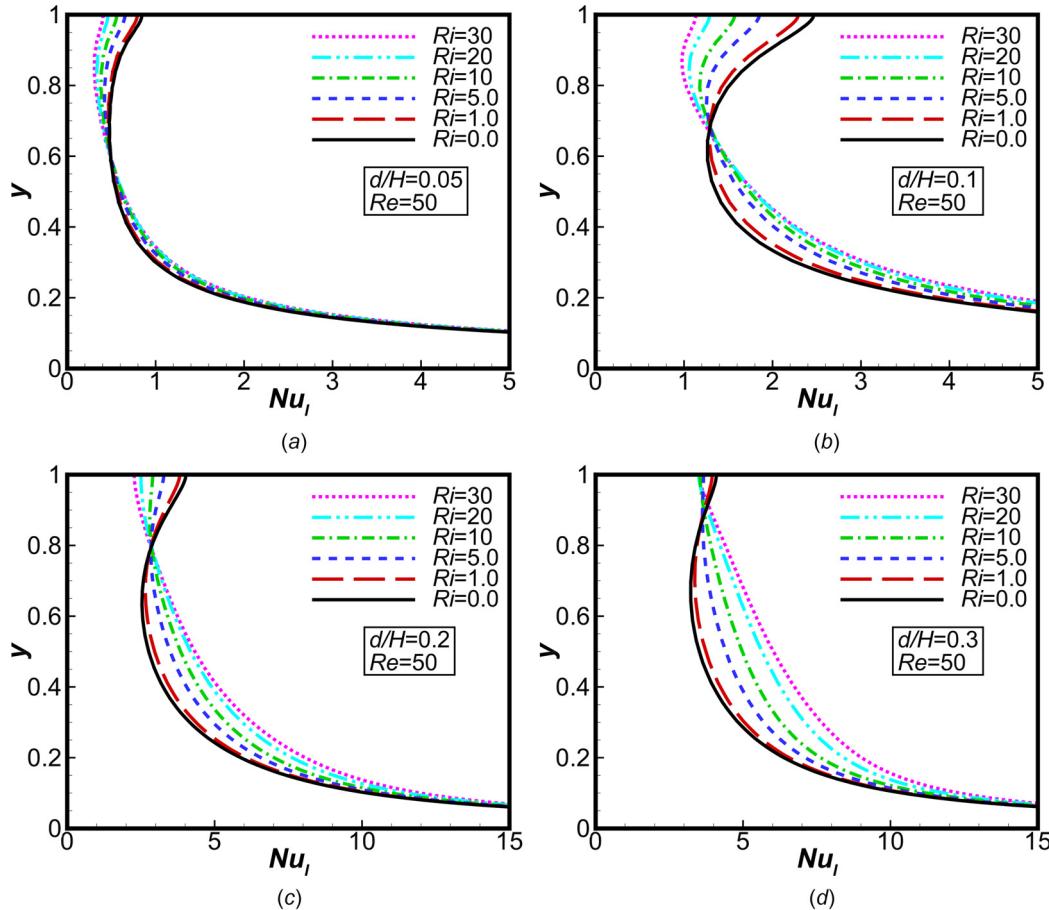
Fig. 9   Variation of Nu_l for different Ri and d/H, at Re = 50; (a) at $d/H = 0.05$; (b) at $d/H = 0.1$; (c) at $d/H = 0.2$; and (d) at $d/H = 0.3$

The streamlines and isotherms patterns presented in Fig. 7 describe the mixed convective flows under various heating regimes at Re = 250 and for (a) d/H = 0.05 and (b) d/H = 0.3, respectively. At d/H = 0.05, when the heating effect is neglected at Ri = 0, a single clockwise vortex is formed by the effect of the mainstream flow (forced convection) inside the enclosure. As Richardson number increases and at Ri = 0.6, it is observed that the intensity of the single vortex increases, inducing a secondary anticlockwise vortex at the lower right corner of the enclosure. With further increase in Richardson number, the lower circulation vortex gets larger and spreads fully in the lower part of the enclosure, and thereby squeezes the primary vortex toward the upper part, resulting of two eddies that have almost the same kinetic energy at Ri = 5.0. However, the jet effect is vanished and not observed at the wider openings d/H = 0.3.

To demonstrate the effect of Reynolds number, streamlines and isotherms patterns for different Re = 50, 75, 100, and 125, at constant Ri = 5.0, are shown in Figs. 8(a) and 8(b) for two values of d/H = 0.05 and 0.3, respectively. In Fig. 8(a), for an inlet nozzle at d/H = 0.05, it is clear that at low Re = 50, the heating effect pushes the primary vortex initially formed in the core of the enclosure toward the top right corner. As Reynolds number increases, the force convective jet assists the moderate buoyancy forces to accelerate the fluid near the hot left wall moving upward, and then producing two clockwise upper-stream and anticlockwise downstream eddies. This bifurcation phenomenon is not observed in Fig. 8(b) for the largest inlet port at d/H = 0.3 as the jet effect vanishes.

The spatial variations of the local rate of heat transfer parameterised by the Nusselt number (Nu_l) along the vertical left heated wall of the enclosure are presented in Figs. 9 and 10 for Re = 50 and 250, respectively, at different opening sizes d/H and

Richardson numbers Ri. The striking characteristic in these figures is that the distributions tend to be arranged in descending order with increasing Richardson number particularly for those at higher opening size. Thus, the highest values are attained at the lower portion of the wall, from which point Nu_l decreases monotonically as the vertical coordinate increases. The peaks in the lower portion of the wall are due to the dominance of the mainstream flow at the inlet port. However, for lower Richardson number, there is a local maximum in Nu_l at an intermediate vertical distance due to the lesser effect of natural convection.

4.2 Effect of Inlet and Outlet Openings. The effectiveness of heat transfer inside the enclosure with varying the size of the opening ports d/H is displayed in Fig. 11 in terms of average Nusselt number (Nu_m) along the hot wall for different Richardson numbers, and at Re = 50, 100, 150, 200, and 250. It is obvious that the values of Nu_m generally increase with increasing the size of ports for all Richardson and Reynolds numbers. Indeed, the effect of increasing the port size becomes more significant at higher Richardson numbers. This is due to the assistance of the buoyancy forces in thinning the boundary layer near the wall and decrease of the average bulk fluid temperature. In addition, the minimum Nu_m is expected to be found at the smallest size of the inlet port at d/H = 0.05. The physical reason behind that is the heating effect is stronger than the effect of incoming forced jet even for higher Reynolds numbers generating a thicker thermal boundary layer close the hot wall. This can be seen in Figs. 7(a) and 8(a) showing the uniform temperature distributions inside the enclosure at d/H = 0.05, for different values of Reynolds and Richardson numbers. Moreover, interestingly, the figure shows that there is an optimal value of the port size, which is at
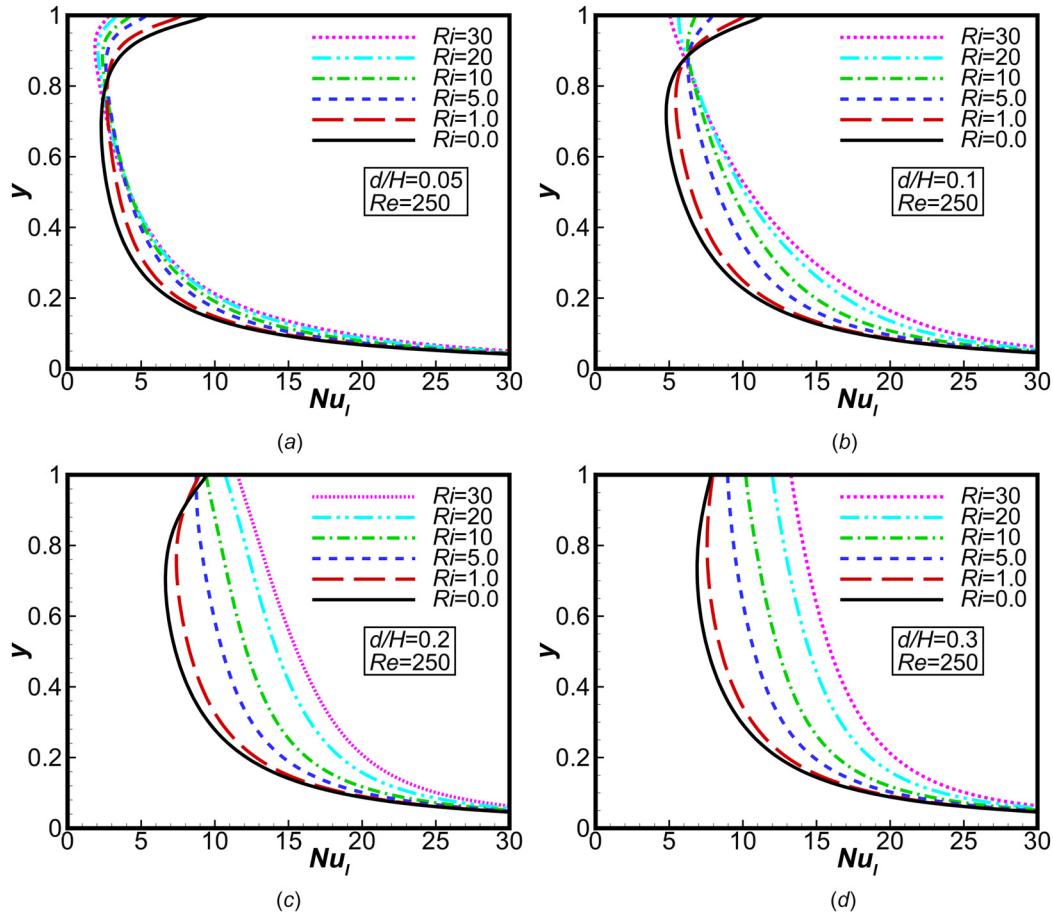
Fig. 10   Variation of Nu_l for different Ri and d/H, at Re = 250; (a) at d/H = 0.05; (b) at d/H = 0.1; (c) at d/H = 0.2; and (d) at d/H = 0.3
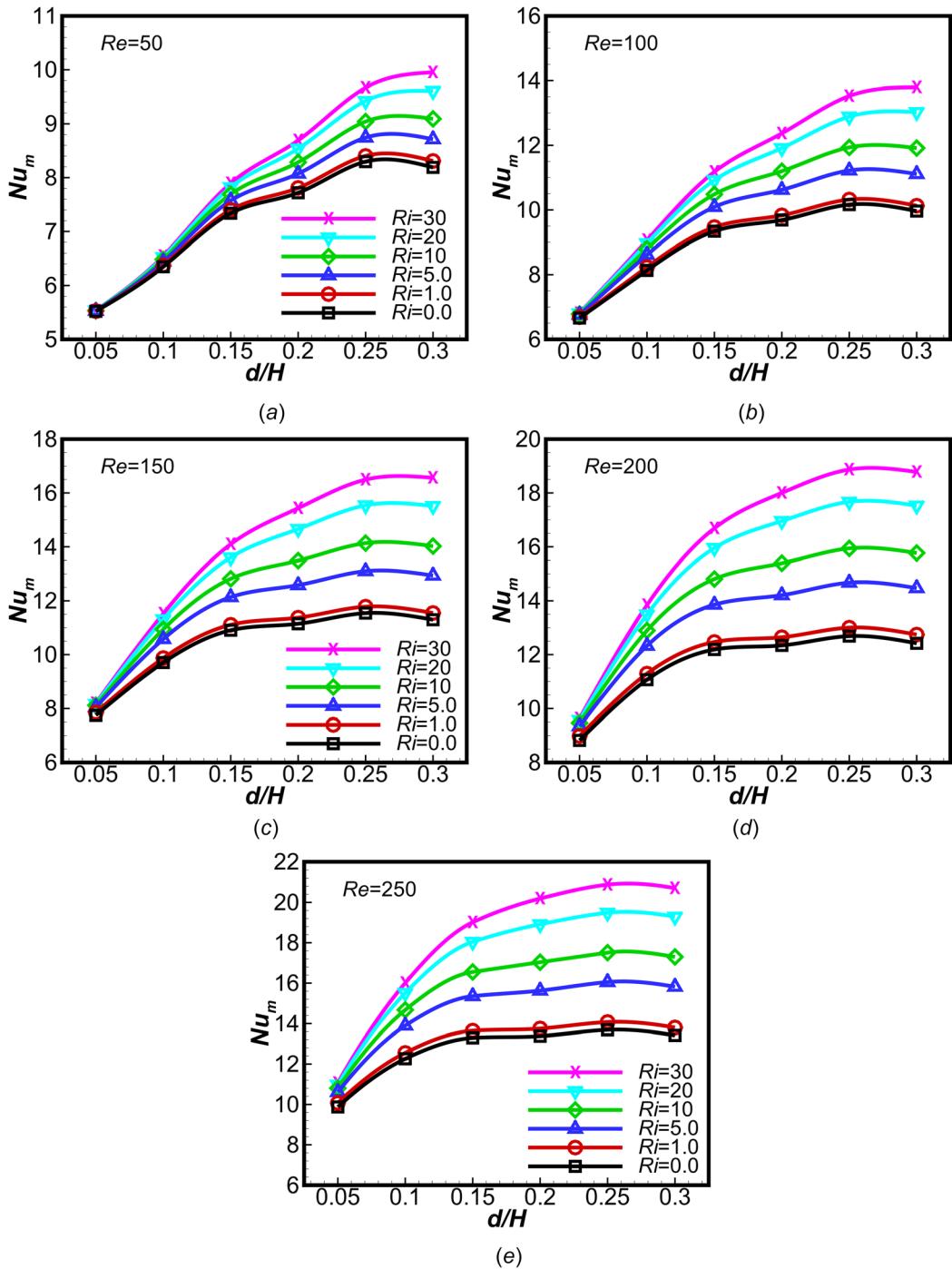
Fig. 11 Effect of *d/H* on Nu_m for different Ri and Re: (*a*) at Re = 50; (*b*) at Re = 100; (*c*) at Re = 150; (*d*) at Re = 200; and (*e*) at Re = 250

$d/H = 0.25$, for acquiring maximum Nu$_m$, thus after this value, there is no benefit from increasing the port size. It is seen that this occurs almost for all values of Richardson and Reynolds numbers. The reason is due to the change in the flow behavior inside the cavity as will be explained in Fig. 12. However, importantly, for particular cases of lower Richardson numbers and higher Reynolds numbers, for instance, for Re $\geq$ 150 and Ri $\leq$ 1.0, one can see that the profiles of Nu$_m$ are approximately kept constant when $d/H > 0.15$.

Figure 12 shows the streamlines and isotherms plots for different port sizes d/H, at Re = 200 and Ri = 30. At $d/H = 0.05$, although a jet-wall-type flow is observed at the inlet opening, the heating influence is dominant in the enclosure, and the buoyancy driven currents form two primary and secondary cells circulating at the top and bottom, , respectively. As the port size increases, the penetration effect of the main flow becomes important. Thus, the interaction between the recirculating zones and the incoming air jet gets stronger, and the primary and secondary cells develop to have same size. The development in the circulating cells is due to the fluid mixing as a result of convective and buoyancy driven currents, consequently, the heat transfer rates increase. This is clear in the corresponding thermal plots as the isotherms significantly propagate from the heated wall toward the enclosure at lower port size; however, a thinner thermal boundary is observed at higher port size. However, it is shown that as the port size increases, the primary recirculating cell in the top region of the

(a) $(d/H) = 0.05$ (b) $(d/H) = 0.1$ (c) $(d/H) = 0.15$

(d) $(d/H) = 0.2$ (e) $(d/H) = 0.25$ (f) $(d/H) = 0.3$

((Isotherms)

(a) $(d/H) = 0.05$ (b) $(d/H) = 0.1$ (c) $(d/H) = 0.15$

(d) $(d/H) = 0.2$ (e) $(d/H) = 0.25$ (f) $(d/H) = 0.3$

0.00 0.07 0.13 0.20 0.27 0.33 0.40 0.47 0.53 0.60 0.67 0.73 0.80 0.87 0.93 1.00
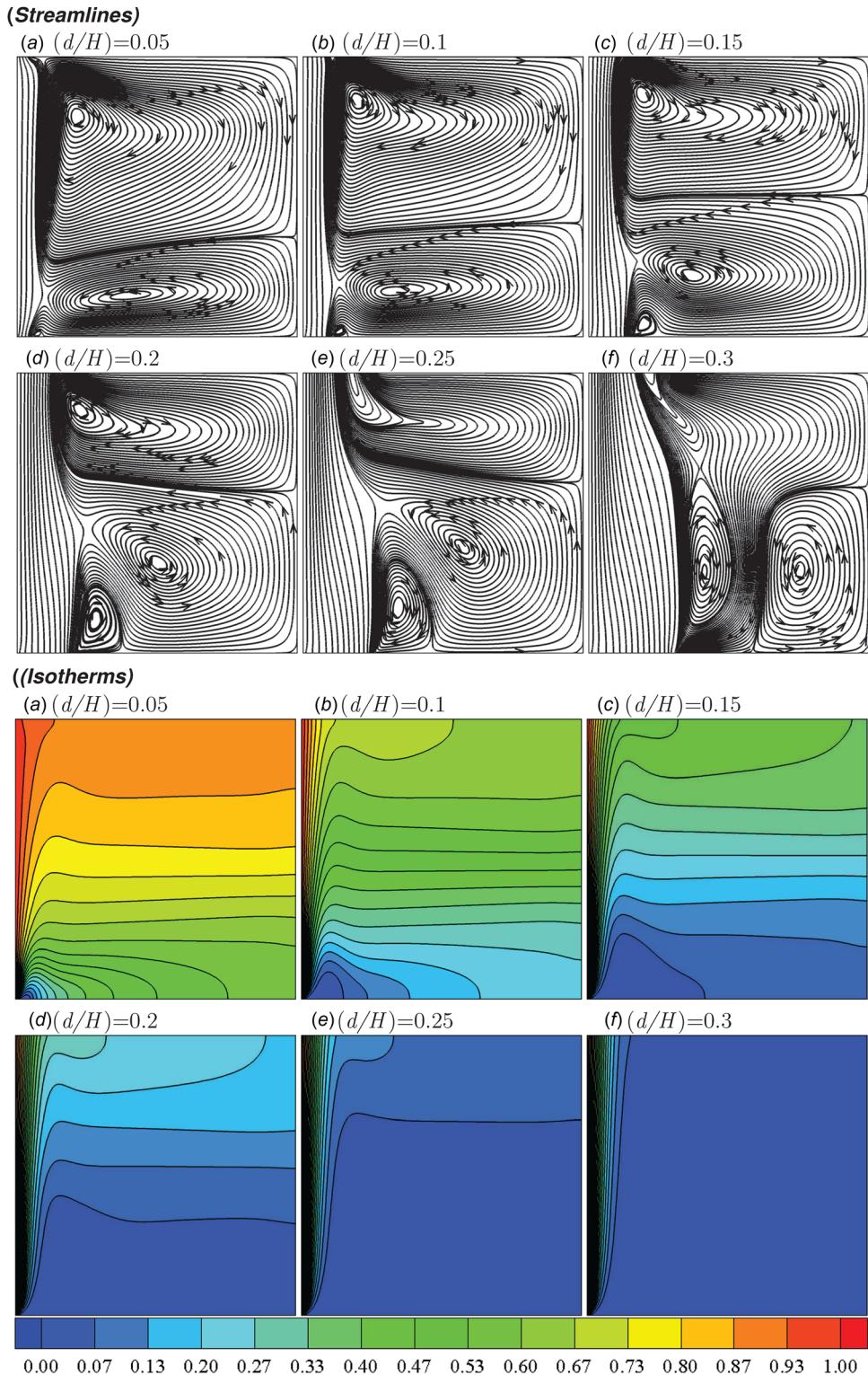
Fig. 12 Effect of *d/H* on the flow behavior represented by the streamlines and the temperature distributions, at Ri = 30 and Re = 200

cavity considerably diminishes, and then vanishes behind $d/H = 0.25$. This behavior assists the thermal boundary layer to get some expansion in this area, and clarifying the reduction in Nu_m behind $d/H = 0.25$ in Fig. 11.

The effect of the three main parameters, namely, Reynolds and Richardson numbers and openings height, on the normalized rate of heat transfer Nu_m is generally depicted in Fig. 13 over their entire examined ranges. It can be seen that Nu_m varies between a

minimum value 5 (blue color) and maximum value 21 (red color). The figure shows that the higher Nu_m can be obtained at higher Reynolds number, higher Richardson number, and/or higher openings height.

4.3 Effect of Inlet/Outlet Openings' Locations. Six various inlet/outlet configurations were investigated for the problem of
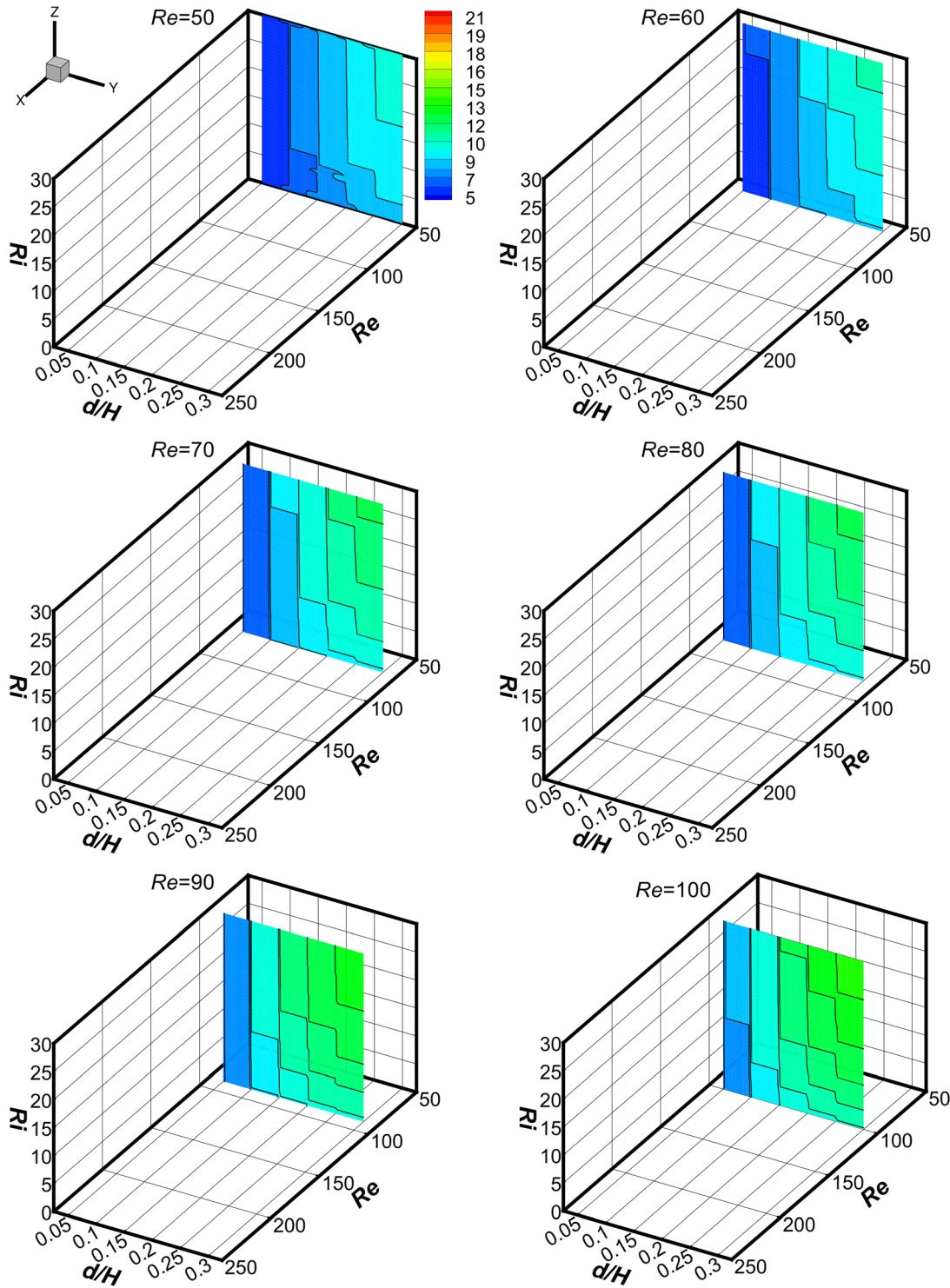
Fig. 13 Influence of three main parameters, Re, Ri, and *d/H*, on Nu$_m$ for the (BLTL1) flow configuration Re = 50 - 250: (*a*) at Re = 50; (*b*) at Re = 100; (*c*) at Re = 150; (*d*) at Re = 200; and (*e*) at Re = 250

mixed convection to compare the behaviors of the convective heat transfer for diverse relative inlet and outlet positions. Figure 14 presents the results of the average Nusselt number Nu$_m$ at the hot wall for all the six configurations, with Richardson number, at Re = 50, 100, 150, 200, and 250. It is observed that the BLTL1 and the BLTR2 configurations are the most desirable configurations that results in higher Nu$_m$ for all values of Richardson and

Reynolds numbers. This occurs when the cold air is injected vertically near the hot wall and exists the enclosure whether from the opposite outlet port (BLTL1) or from that one moving away from the hot wall (BLTR2). This is due to the injection effect of the cold stream along the hot wall, and the forced and natural convections assist each other in these configuration. Therefore, it is seen that higher heat transfer rates are obtained at higher Richardson
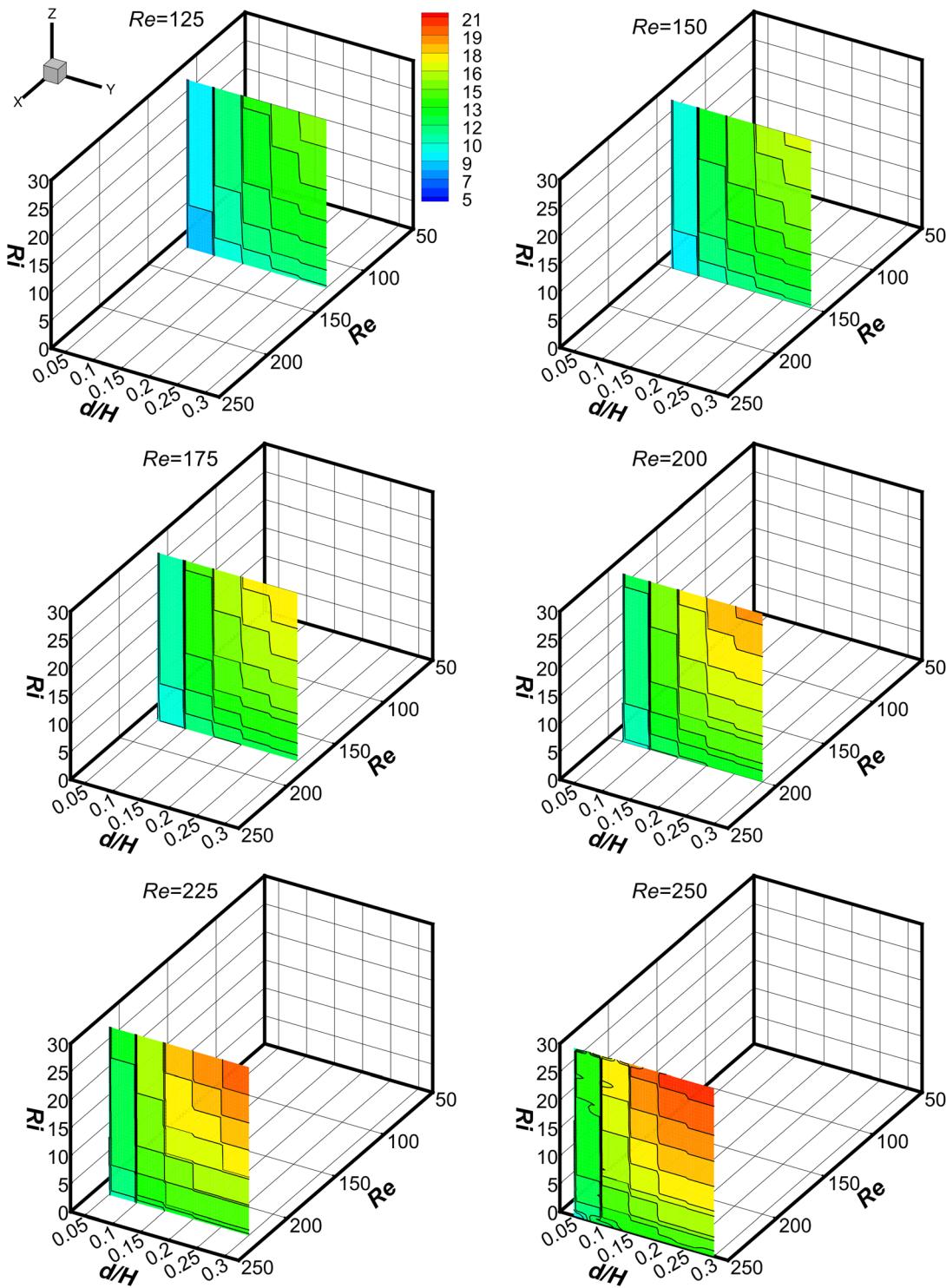
Fig. 13 (Continued)

number and/or higher Reynolds number. The figure also shows that Nu_m for the (BLTL1) configuration is always slightly higher than other configurations, except for $Ri \leq 10$ at $Re = 50$, due to the dominance of natural convection.

The next two beneficial configurations are the BRTL3 and the BRTR4, when the inlet opening is placed through the bottom but away from the heated wall and the exit is located in the opposite through the top. It is observed that these arrangements give much lesser heat removal than the (BLTL1) and (BLTR2) for the whole

Richardson and Reynolds numbers. Also, Nu_m for the (BRTL3) arrangement is always considerably higher than that for the (BRTR4) arrangement. It also seems that the forced convection and the natural convection aid each other but after a strong conflict between the flows generated by inertia and buoyancy forces in the enclosure.

In contrast, the remaining inlet/outlet configurations, namely, the bottom-left-bottom-right (BLBR5) and the bottom-right-bottom-left (BRBL6) when both inlet and outlet ports are located
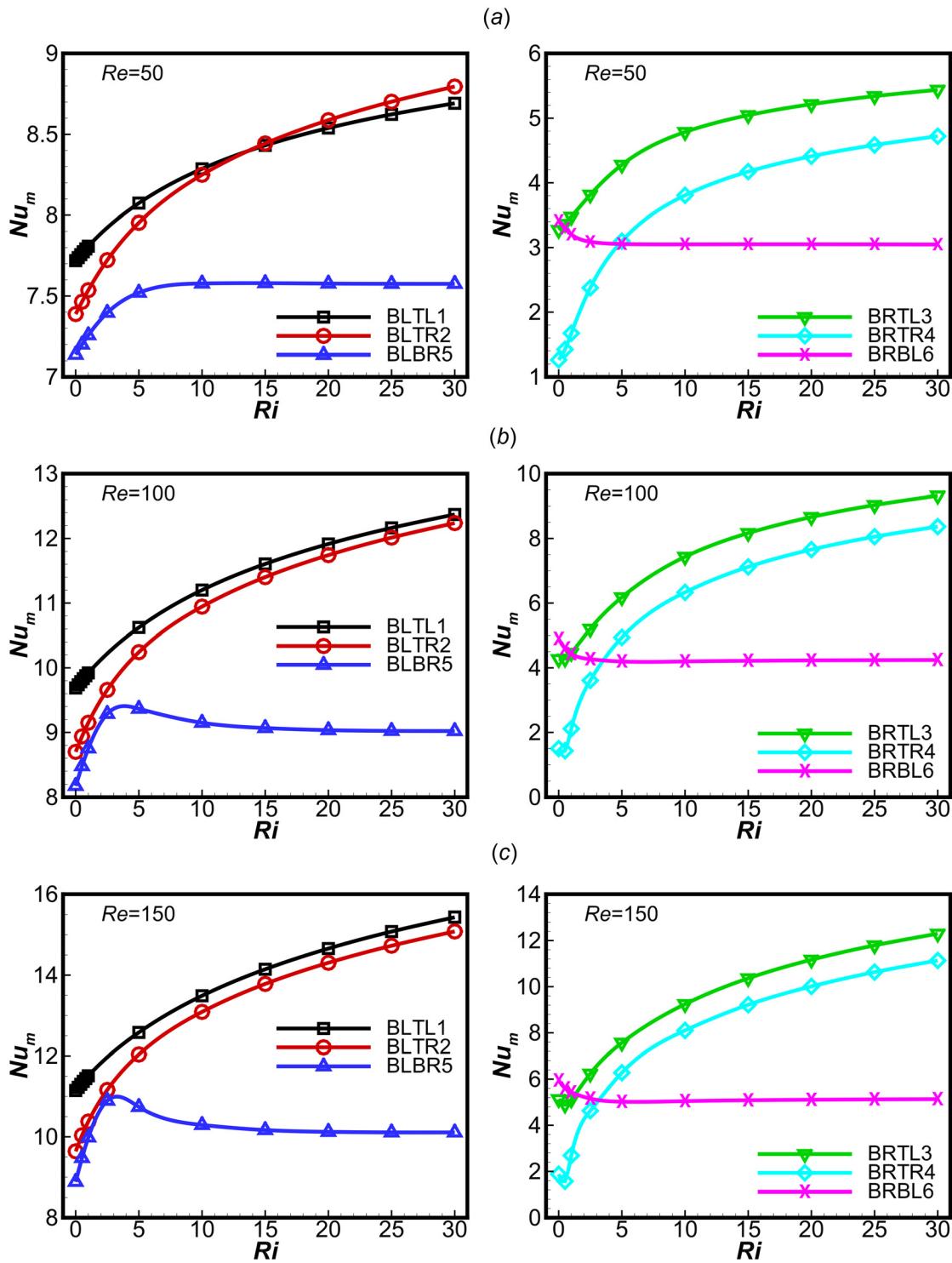
Fig. 14 Effect of different enclosure configurations on Nu_m at *d/H* = 0.2 and for different Re = 50, 100, 150, 200, and 250

through the bottom, are unfavorable to the natural convection phenomenon. Thus, the Nu_m curves are almost flat for Ri ≤ 5, when the natural convection becomes dominant. Also, there is a decreasing tendency observed before that in the (BRBL6) configuration, which is found to be the worst flow configuration for most of the cases. This is could be due to the complex structure of flow which is not favorable to the formation of the big circulating cells inside the enclosure. However, interestingly, it is shown that Nu_m

for the (BLBR5) configuration is higher than that for the (BRTL3) and (BRTR4) configurations but only at moderate and lower values of Richardson and Reynolds numbers.

As a consequence of space limitation, it is impossible to comprise the results for all the six configurations for all Richardson and Reynolds numbers. Therefore, some representative streamlines and isotherms are presented in Figs. 15 and 16 for all the enclosure displacement configurations at only two values of
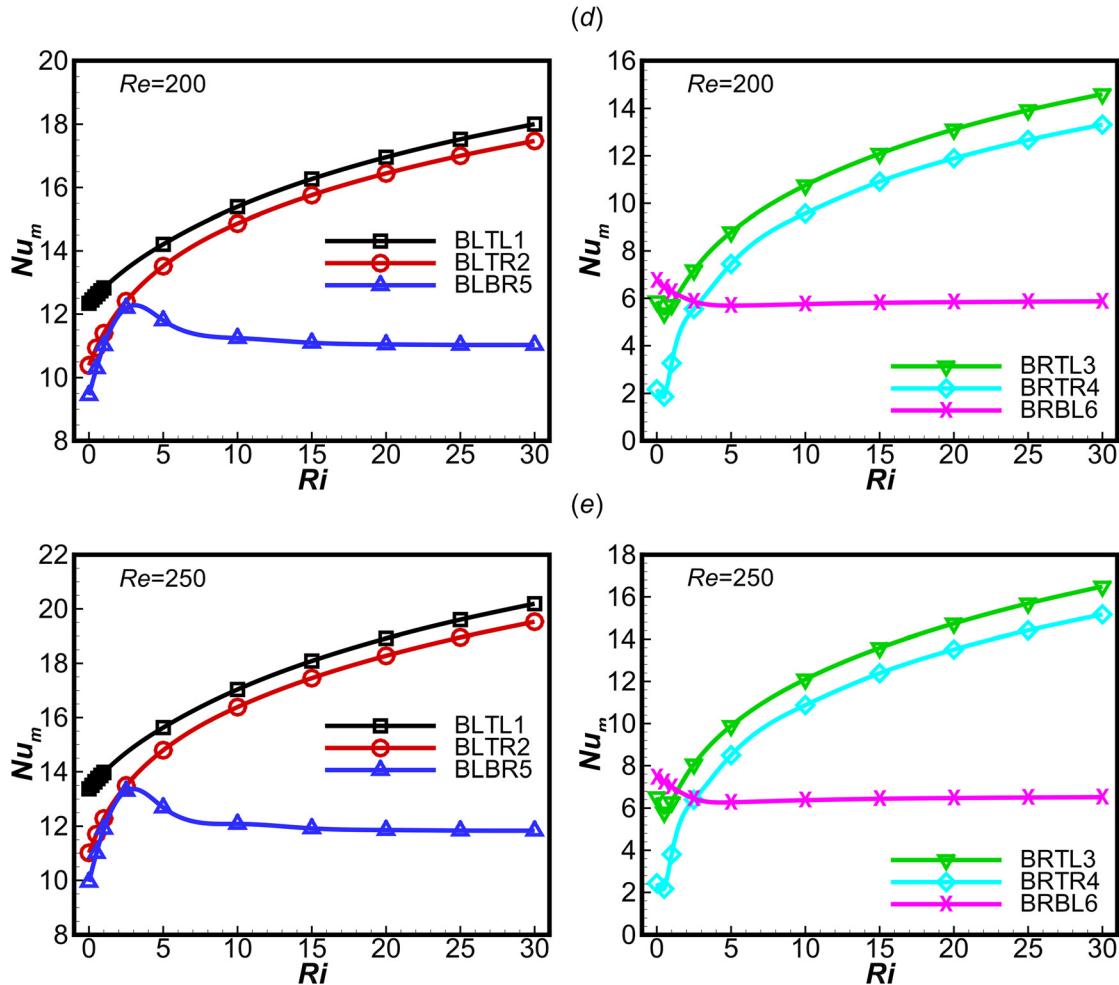
Fig. 14 (Continued)

$\text{Re} = 50$ and 250, respectively, and at $\text{Ri} = 30$. Close scrutiny of these dynamic and thermal fields tells the phenomena of heat transfer in the enclosure for the corresponding configuration. It can be seen that as Reynolds number increases, a severe competition between the inertia forces and the flow produced by buoyancy is clearly observed. Then, a variety of sophisticated mixed-convection flow structures and physics is generated. Also, open lines of the external forced flow are shown to occupy nearly the entire enclosure at $\text{Re} = 50$. Most of these open lines are without being aspired by the heated wall, and a closed shear cell is formed under the open lines. The corresponding isotherms display a fine thermal stratification over the enclosure space, leading to zero gradients of temperature in the horizontal direction. For the higher value of $\text{Re} = 250$ and the higher value of $\text{Ri} = 30$, there is an increase in the intensity of the internal flow support the formation of at least two nonuniform cells within the cavity. The external flow interacts strongly with the heated wall by reason of the high jet velocities, and the corresponding isotherms demonstrate that the thermal stratification is reduced considerably, except for the (BLBR5) and (BRBL6), and the heat exchange is increased.

5 Conclusions

A numerical study has been conducted to investigate laminar combined forced and natural convection heat transfer characteristics inside a vertical heated enclosure. The effects of inlet/outlet ports size and location have been examined for broad ranges of Reynolds and Richardson numbers. Six possible placement configurations of the inlet and outlet, namely, BLTL1, BLTR2, BRTL3, BRTR4, BLBR5, and BRBL6, have been studied. The study was made using a two-dimensional computational model developed using the finite volume formulation. The in-house code is validated and verified with the results available in the literature. Results of the study show that the increase in Reynolds number and/or Richardson number increases the average Nusselt number (Nu_m). The influence of the increase in Richardson number becomes more significant for higher openings size and higher Reynolds number. In addition, the results show that Nu_m increases with increasing the openings size for all values of Richardson and Reynolds numbers. In addition, the effect of opening height being important at higher Richardson number; however, it is trivial for $d/H > 0.15$ at lower Richardson number and higher Reynolds number. Also, it is found that the maximum Nu_m occurs when $d/H = 0.25$ for the entire values of Richardson and Reynolds numbers, while the minimum Nu_m happens at the smallest port size of $d/H = 0.05$. Moreover, the (BLTL1) configuration and then the (BLTR2) are found to be the most desirable arrangements for the inlet and outlet locations that results in higher Nu_m at all conditions. However, the (BLBR5) and the (BRBL6) configurations, when both the inlet and the outlet ports are located at the same bottom side, are the worst unfavorable flow distributions for most of Reynolds and Richardson cases.

(*Streamlines*)

(*a*)(*BLTL1*)   (*b*)(*BLTR2*)   (*c*)(*BRTL3*)

(*d*)(*BRTR4*)   (*e*)(*BLBR5*)   (*f*)(*BRBL6*)

(*Isotherms*)

(*a*)(*BLTL1*)   (*b*)(*BLTR2*)   (*c*)(*BRTL3*)

(*d*)(*BRTR4*)   (*e*)(*BLBR5*)   (*f*)(*BRBL6*)

0.00 0.07 0.13 0.20 0.27 0.33 0.40 0.47 0.53 0.60 0.67 0.73 0.80 0.87 0.93 1.00
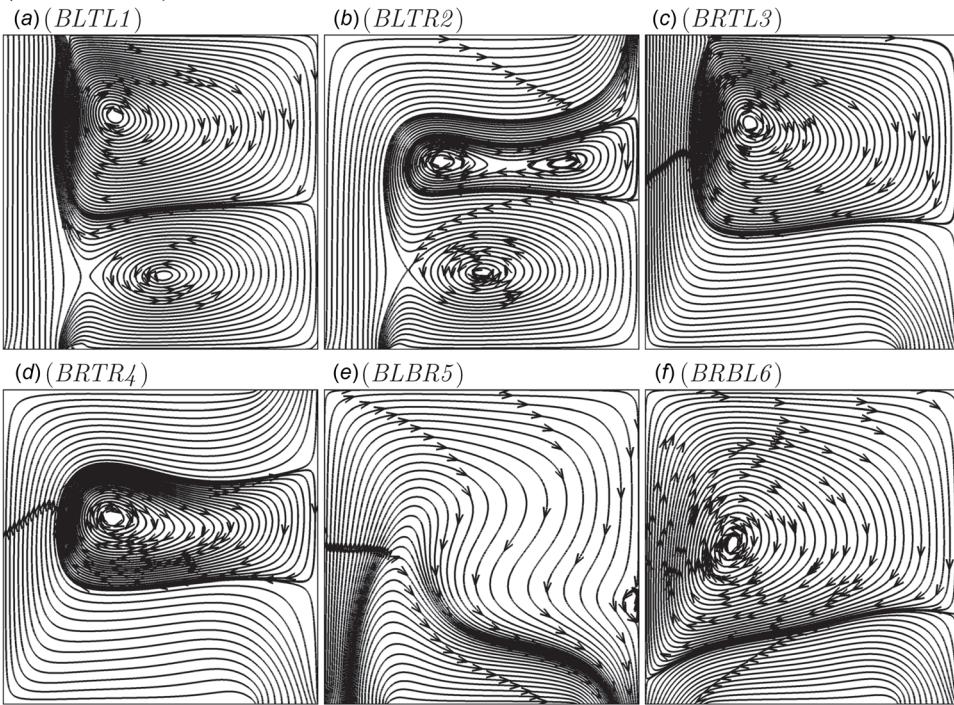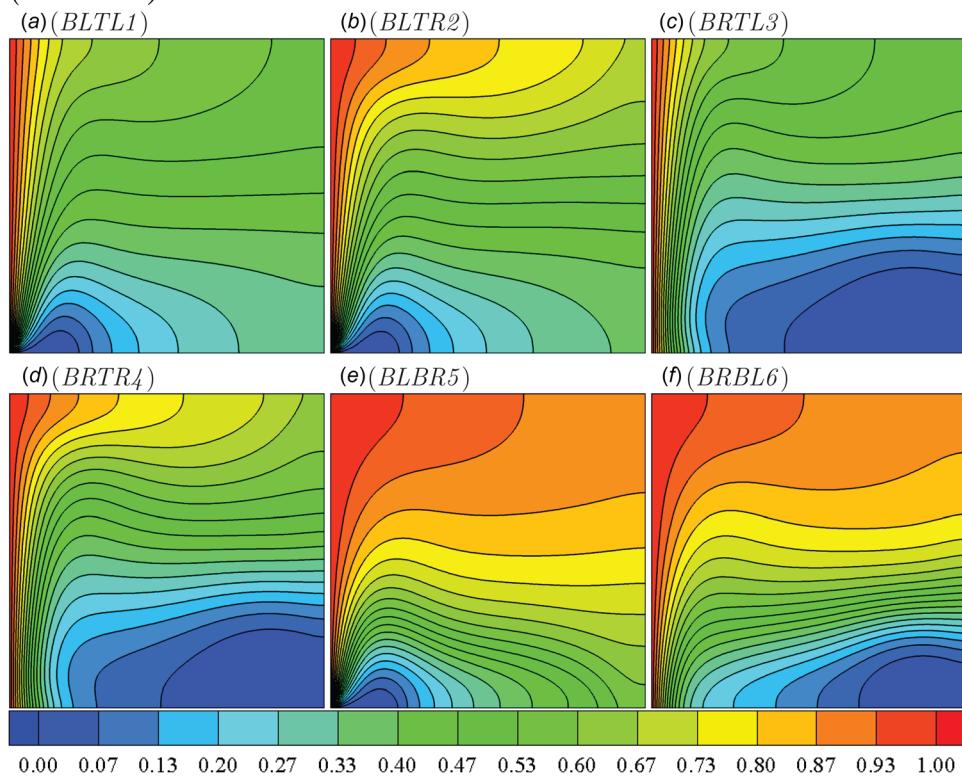
Fig. 15 Effect of different enclosure configurations on the streamlines and isotherms $d/H = 0.2$, Ri = 30, and Re = 50
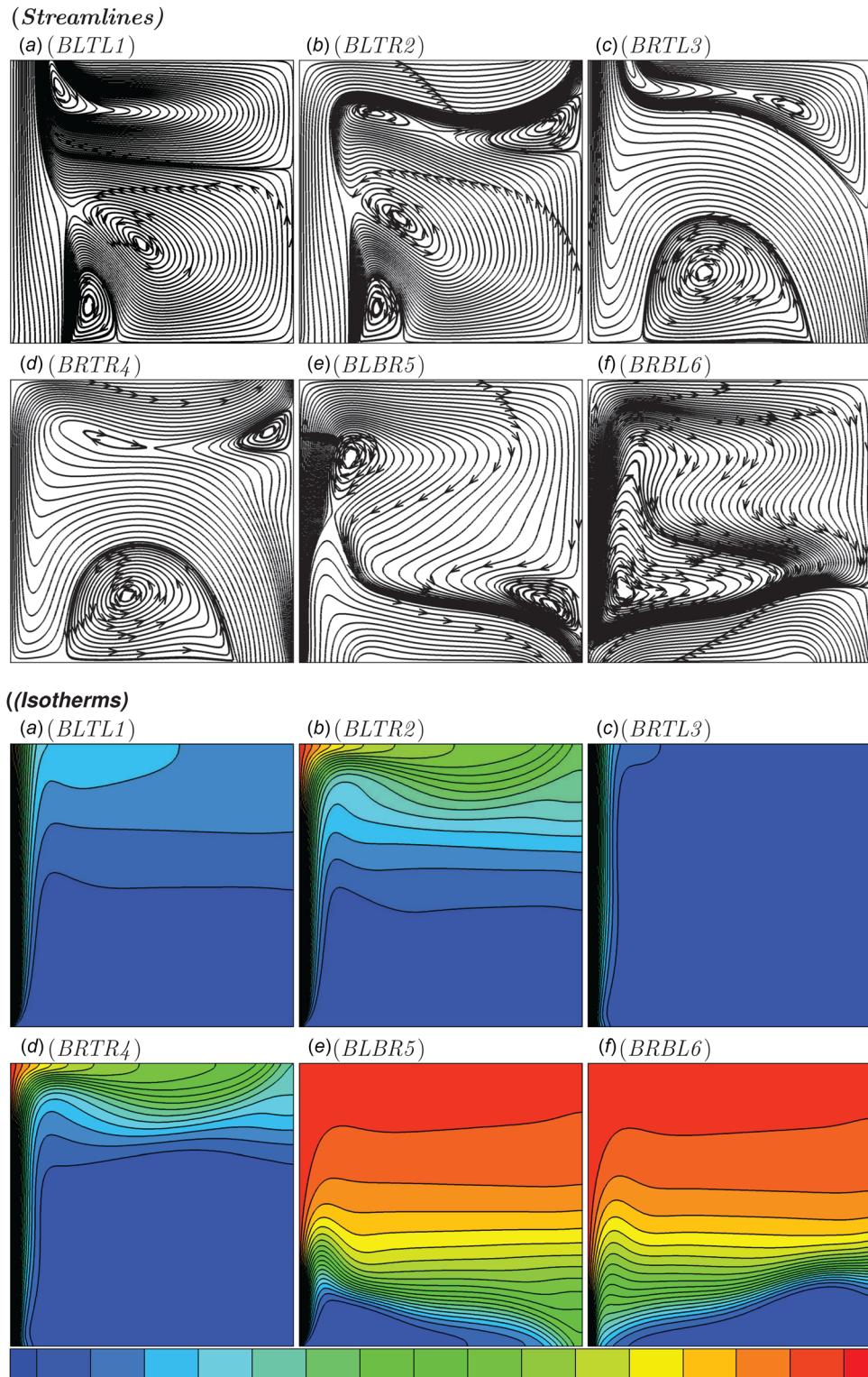
Fig. 16 Effect of different enclosure configurations on the streamlines and isotherms $d/H = 0.2$, $\mathrm{Ri} = 30$, **and Re = 250**

Nomenclature

d = enclosure inlet slot or outlet vent height (m)

Gr = Grashof number, $\mathrm{Gr} = g \cdot \beta \cdot H^3 \cdot (T_w - T_o)/\nu^2$

H = enclosure height (m)

$\mathrm{Nu_l}$ = local mean-time surface-average Nusselt number

$\mathrm{Nu_m}$ = time- and surface-average Nusselt number

P = dimensionless pressure
Pr = Prandtl number, Pr = ν/α
Re = Reynolds number, Re = $v_{\mathrm{o}}.H/\nu$
Ri = Richardson number, Ri = $\mathrm{Gr}/\mathrm{Re}^2$
t = dimensionless time
u = dimensionless horizontal velocity
v = dimensionless vertical velocity
w = wall
x, y = dimensionless Cartesian coordinates

Greek Symbols

β = volumetric expansion coefficient
θ = dimensionless temperature, $\theta = (T - T_{\mathrm{o}})/(T_{\mathrm{w}} - T_{\mathrm{o}})$
ν = kinematic viscosity (m^2/s)
ρ = density (kg/m^3)

References

[1] Papanicolaou, E., and Jaluria, Y., 1991, "Mixed Convection From an Isolated Heat Source in a Rectangular Enclosure," Numer. Heat Transfer, Part A, **18**(4), pp. 427–461.

[2] Papanicolaou, E., and Jaluria, Y., 1992, "Transition to a Periodic Regime in Mixed Convection in a Square Cavity," J. Fluid Mech., **239**(1), pp. 489–509.

[3] Hsu, T., Hsu, P., and How, S., 1997, "Mixed Convection in a Partially Divided Rectangular Enclosure," Numer. Heat Transfer, Part A, **31**(6), pp. 655–683.

[4] Raji, A., and Hasnaoui, M., 1998, "Mixed Convection Heat Transfer in a Rectangular Cavity Ventilated and Heated From Side," Numer. Heat Transfer, Part A, **33**(5), pp. 533–548.

[5] Raji, A., and Hasnaoui, M., 2000, "Mixed Convection Heat Transfer in Ventilated Cavities With Opposing and Assisting Flows," Eng. Comput., **17**(5), pp. 556–572.

[6] Lee, S. C., Cheng, C. Y., and Chen, C. K., 1997, "Finite Element Solutions of Laminar and Turbulent Flows With Forced and Mixed Convection in an Air-Cooled Room," Numer. Heat Transfer, Part A, **31**(5), pp. 529–550.

[7] Moraga, N. O., and Lopez, S. E., 2004, "Numerical Simulation of Three-Dimensional Mixed Convection in an Air-Cooled Cavity," Numer. Heat Transfer, Part A, **45**(8), pp. 811–824.

[8] Doghmi, H., Abourida, B., Belarche, L., Sannad, M., and Ouzaouit, M., 2018, "Effect of the Inlet Opening on Mixed Convection Inside a 3-D Ventilated Cavity," Therm. Sci., **22**(6 Pt A), pp. 2413–2424.

[9] Omri, A., and Ben Nasrallah, S., 1999, "Control Volume Finite Element Numerical Simulation of Mixed Convection in an Air-Cooled Cavity," Numer. Heat Transfer, Part A, **36**(6), pp. 615–637.

[10] Singh, S., and Sharif, M. A. R., 2003, "Mixed Convective Cooling of a Rectangular Cavity With Inlet and Exit Openings on Differentially Heated Side Walls," Numer. Heat Transfer, Part A, **44**(3), pp. 233–253.

[11] Rahman, M. M., Alim, M. A., Mamun, A. H., Chowdhury, M. K., and Islam, A. K., 2007, "Numerical Study of Opposing Mixed Convection in a Vented Enclosure," ARPN J. Eng. Appl. Sci., **2**(2), pp. 25–36.

[12] Bahlaoui, A., Raji, A., Hasnaoui, M., Naïmi, M., Makayssi, T., and Lamsaadi, M., 2009, "Mixed Convection Cooling Combined With Surface Radiation in a Partitioned Rectangular Cavity," Energy Convers. Manage., **50**(3), pp. 626–635.

[13] Oztop, H. F., 2010, "Influence of Exit Opening Location on Mixed Convection in a Channel With Volumetric Heat Sources," Int. Commun. Heat Mass Transfer, **37**(4), pp. 410–415.

[14] Nosonov, I. I., and Sheremet, M. A., 2018, "Conjugate Mixed Convection in a Rectangular Cavity With a Local Heater," Int. J. Mech. Sci., **136**, pp. 243–251.

[15] Sparrow, E. M., and Samie, F., 1982, "Interaction Between a Stream Which Passes Through an Enclosure and Natural Convection Within the Enclosure," Int. J. Heat Mass Transfer, **25**(10), pp. 1489–1502.

[16] Oosthuizen, P. H., and Paul, J. T., 1985, "Mixed Convection Heat Transfer in a Cavity," Fundamentals of Forced and Mixed Convection (Heat Transfer Division), F. A. Kulacki, and D. B. Ronald, eds., Vol. 42, American Society of Mechanical Engineers, New York, pp. 159–169.

[17] Kumar, R., and Yuan, T., 1989, "Recirculating Mixed Convection Flows in Rectangular Cavities," J. Thermophys. Heat Transfer, **3**(3), pp. 321–329.

[18] Angirasa, D., 2000, "Mixed Convection in a Vented Enclosure With an Isothermal Vertical Surface," Fluid Dyn. Res., **26**(4), pp. 219–233.

[19] Patankar, S. V., 1980, Numerical Heat Transfer and Fluid Flow, Hemisphere Publishing Corporation, New York.

[20] Ferziger, J. H., and Peric, M., 1997, Computational Methods for Fluid Dynamics, Springer, Berlin.